A vertebrate N-end rule degron reveals that Orc6 is required in mitosis for daughter cell abscission

Juan A. Bernal and Ashok R. Venkitaraman

Medical Research Council Cancer Cell Unit, Hutchison/Medical Research Council Research Centre, Cambridge CB2 0XZ, England, UK

Orc6, an evolutionarily conserved component of the origin recognition complex, is essential for deoxyribonucleic acid (DNA) replication initiation from yeast to humans. Whether vertebrate Orc6 has a mitotic function remains unresolved. In vertebrates, but not yeast, its depletion causes centrosome amplification and multinucleate division, but replication stress indirectly causes similar abnormalities. In this paper, we exploit Varshavsky's N-end rule to create a temperature-sensitive degron form of avian Orc6. Orc6 depletion during the S phase triggers centrosome amplification suppressed by G2 checkpoint inhibition, reflecting an indirect consequence of aberrant DNA replication. However, Orc6 depletion during mitosis suffices to cause asymmetric division and failure in cytokinesis, with a delay in daughter cell abscission revealed by a fluorescence-bleaching assay. A mutant lacking the C-terminal 25 residues cannot rescue these defects. Thus, vertebrate Orc6 is necessary during mitosis for the abscission stage of cytokinesis. Our findings exemplify N-end rule degrons as tools to unravel functions of a single protein during different phases of the vertebrate cell cycle.

Introduction

Origin recognition complex proteins form a hexameric complex that helps to load replication initiation factors at origins of replication (Bell and Stillman, 1992; Rowles and Blow, 1997; Quintana and Dutta, 1999). Orthologues occur in *Saccharomyces cerevisiae* (Li and Herskowitz, 1993), *Drosophila melanogaster* (Gossen et al., 1995), *Xenopus laevis* (Gillespie et al., 2001), or *Homo sapiens* (Dhar and Dutta, 2000) and probably exist in all eukaryotes. Orc1–Orc6 are essential for the initiation of DNA replication in all systems so far tested (Duncker et al., 2009) but may also have additional biological functions (Bell et al., 1995; Pak et al., 1997; Bell, 2002; Prasanth et al., 2004; Shimada and Gasser, 2007). The most striking example is Orc6 (Prasanth et al., 2002; Chesnokov, 2007), which has no homology with the other origin recognition complex proteins and has rapidly diverged from budding yeast to humans (Dhar and Dutta, 2000).

Mammalian Orc6 has been implicated in mitosis because its depletion using RNAi causes centrosome amplification and multinuclear cell division (Prasanth et al., 2002). However, Orc6 depletion from asynchronously dividing cells triggers delayed and diverse mitotic phenotypes whose prominence depends on the duration of RNAi treatment. Genetic experiments in budding yeast fail to identify a corresponding role (Semple et al., 2006). Moreover, aberrant replication can itself induce G2 checkpoint activation (Dodson et al., 2004), which when persistent, provokes both centrosome amplification and abnormal cell division (Meraldi et al., 2002). Thus, whether the mitotic abnormalities triggered by mammalian Orc6 depletion reflect direct functions of the protein or are simply the indirect consequences of defective replication remains unresolved. To address this issue, we created a temperature-sensitive N-end rule degron form of vertebrate Orc6 (degron-Orc6) in the avian DT40 cell line using a method we have recently established (Su et al., 2008).

Results and discussion

We made DT40 cells in which endogenous *Orc6* was replaced by *degron-Orc6* using the approach described in Fig. S1 (Su et al., 2008) to fuse endogenous *Orc6* in frame at its 5′ end to a FLAG tag and a thermosensitive N-end rule mutant of

Correspondence to Ashok R. Venkitaraman: arv22@cam.ac.uk

J.A. Bernal's present address is Dept. de Desarrollo Cardiovascular y Reparación, Centro Nacional de Investigaciones Cardiovasculares, Madrid CP28029, Spain.

Abbreviations used in this paper: ANOVA, analysis of variance; KIF, knockin forward; KIR, knockin reverse; KOF, knockout forward; KOR, knockout reverse; MFI, mean fluorescence intensity; Nz, nocodazole.

The Rockefeller University Press $30.00
J. Cell Biol. Vol. 192 No. 6 969–978
www.jcb.org/cgi/doi/10.1083/jcb.201008125

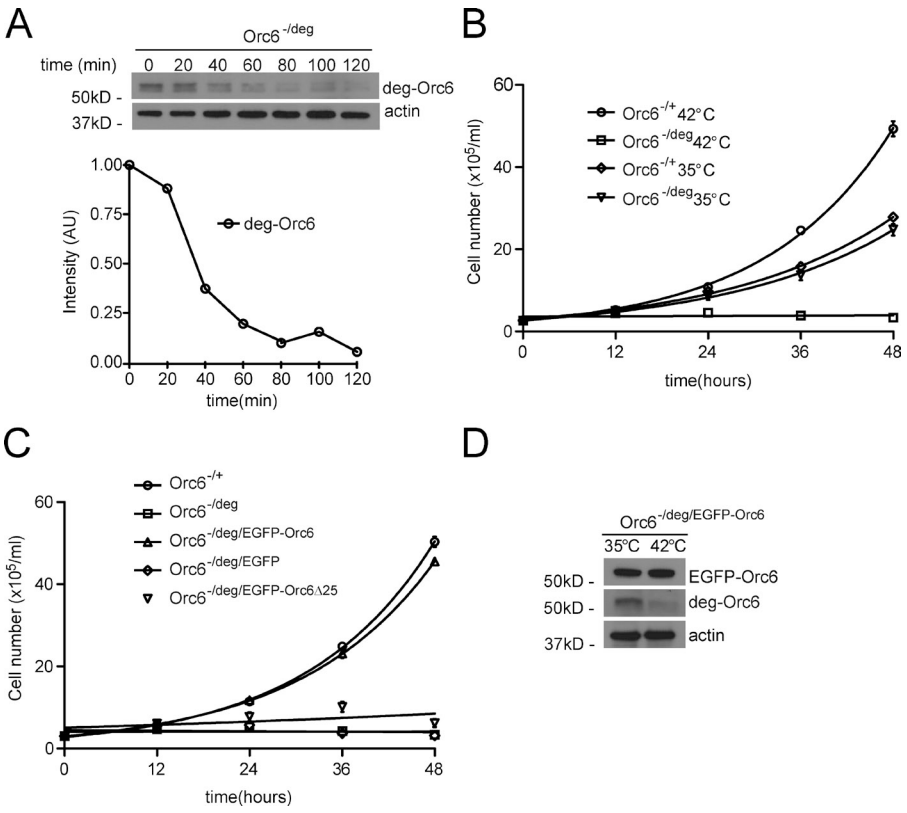

Figure 1. **A thermosensitive N-end rule degron form of vertebrate Orc6 functionally replaces the endogenous protein.** (A) Degron-Orc6 in total cell extracts from *Orc6*$^{-/deg}$ cells is stable at 35°C but undergoes degradation at the nonpermissive temperature 42°C. β-Actin was used as a loading control. Degron-Orc6 immunoblots are shown above a plot showing protein levels in arbitrary units (AU) measured by densitometry on the vertical axis against time. Protein levels were normalized to expression at 0 min and 35°C. (B) Degron-Orc6 in *Orc6*$^{-/deg}$ cells supports viability and cell growth at a similar rate as control cells (doubling time ∼13 h) at 35°C but not at 42°C. The number of viable cells is plotted on the vertical axis against time. (C) Depletion of degron-Orc6 at 42°C results in growth arrest. Reexpression of EGFP-Orc6 (Orc6$^{-/deg/EGFP\text{-}Orc6}$) rescued cell growth, in contrast to EGFP alone (Orc6$^{-/deg/EGFP}$) or EGFP-Orc6Δ25 (Orc6$^{-/deg/EGFP\text{-}Orc6\Delta25}$). (B and C) Data points show the means ± SEM of three independent experiments. (D) Immunoblots showing changes in degron-Orc6 protein levels when shifted to 42°C in Orc6$^{-/deg/EGFP\text{-}Orc6}$ cells. In contrast, the EGFP-Orc6 protein remains stable. β-Actin was used as a loading control.

dihydrofolate reductase (Dohmen et al., 1994; Labib et al., 2000; Dohmen and Varshavsky, 2005). In cells exclusively expressing degron-Orc6 (*Orc6*$^{-/deg}$), the fusion protein is rapidly degraded to <10% of its initial levels within 90 min when cells are shifted from a permissive temperature of 35°C to a nonpermissive temperature of 42°C (Fig. 1 A). Several lines of evidence confirm that degron-Orc6 functionally replaces endogenous Orc6. The viability and proliferation of *Orc6*$^{-/deg}$ cells is similar to that of controls (Fig. 1 B) at 35°C. However, when shifted to 42°C, *Orc6*$^{-/deg}$ cells fail to survive. Complementation with an EGFP-Orc6 fusion protein (which is similar in size to the degron-Orc6 fusion protein but thermostable at 42°C; Fig. 1 D) was sufficient to revert this phenotype (Fig. 1 C). This confirms that the death of *Orc6*$^{-/deg}$ cells at 35°C is a direct effect of Orc6 depletion. Interestingly, complementation with EGFP-Orc6Δ25, a mutant lacking an evolutionarily conserved domain spanning the C-terminal 25 residues of Orc6 (Balasov et al., 2009), did not rescue cell viability (Fig. 1 C).

To define the consequences of Orc6 deficiency during DNA replication, we conditionally depleted degron-Orc6 from cells synchronously released into the S phase of the cell cycle. Centrosome number increased sharply from 16 h after degron-Orc6 depletion (22.8 ± 2.9% vs. control 6.6 ± 2.2%; Fig. 2 A), just as after depletion of the DNA recombinase RAD51 (Fig. S2). Staining with β-tubulin, pericentrin, or γ-tubulin (Fig. 2 B) detected multipolar spindles and supernumerary centrosomes 24 h after degron-Orc6 depletion (79.8 ± 4.7%, mean ± SEM), which were absent from *Orc6*$^{+/-}$ parental cells at 42°C or *Orc6*$^{-/deg}$ control cells at 35°C (9.8 ± 1.9% and 5.6 ± 1%, respectively). The 16–24-h interval after S-phase release when these anomalies occur corresponds to ∼1.5–2 times the typical 10-h doubling time of DT40 cells (Li and Dodgson, 1995), which is indicative of cell cycle prolongation. Indeed, the fraction of degron-Orc6–depleted cells with 4N DNA content increased from 25 to 66% over 24 h (Fig. 2 C), but there was no increase in M-phase cells stained with anti-MPM2 (1.3% at 24 h). Thus, these observations suggest that degron-Orc6 depletion during DNA replication causes arrest in the G2 phase, allowing the accumulation of supernumerary centrosomes and multipolar spindles.

Supporting this notion, phosphorylated Chk1, a G2 checkpoint effector that is induced by defective replication (Heffernan et al., 2002; Xiao et al., 2003), accumulated in degron-Orc6–depleted cells (Fig. 2 D). Treatment of degron-Orc6–depleted cells with caffeine, an inhibitor of G2 checkpoint kinases known to bypass G2 arrest, decreased the percentage of 4N cells from 66 to 42% after 24 h; it correspondingly reduced supernumerary centrosomes and multipolar spindle formation between 16 and 20 h after degron-Orc6 depletion (Fig. 2 E). Finally, cells synchronized with the microtubule poison nocodazole (Nz; Fig. 2 F) before release into mitosis without degron-Orc6 did not exhibit supernumerary centrosome formation (Fig. 2 G). Collectively, these findings argue against a direct role of Orc6 in centrosome duplication or mitotic spindle formation and suggest instead that the occurrence of centrosome and spindle anomalies in degron-Orc6–depleted cells is the result of persistent G2 arrest after defective DNA replication.

Does Orc6 have a direct role in cytokinesis independent of its role in DNA replication? To answer this question, we depleted degron-Orc6 from Nz-arrested cells by incubation at 42°C before release into mitosis (as in Fig. 2 F). Representative frames

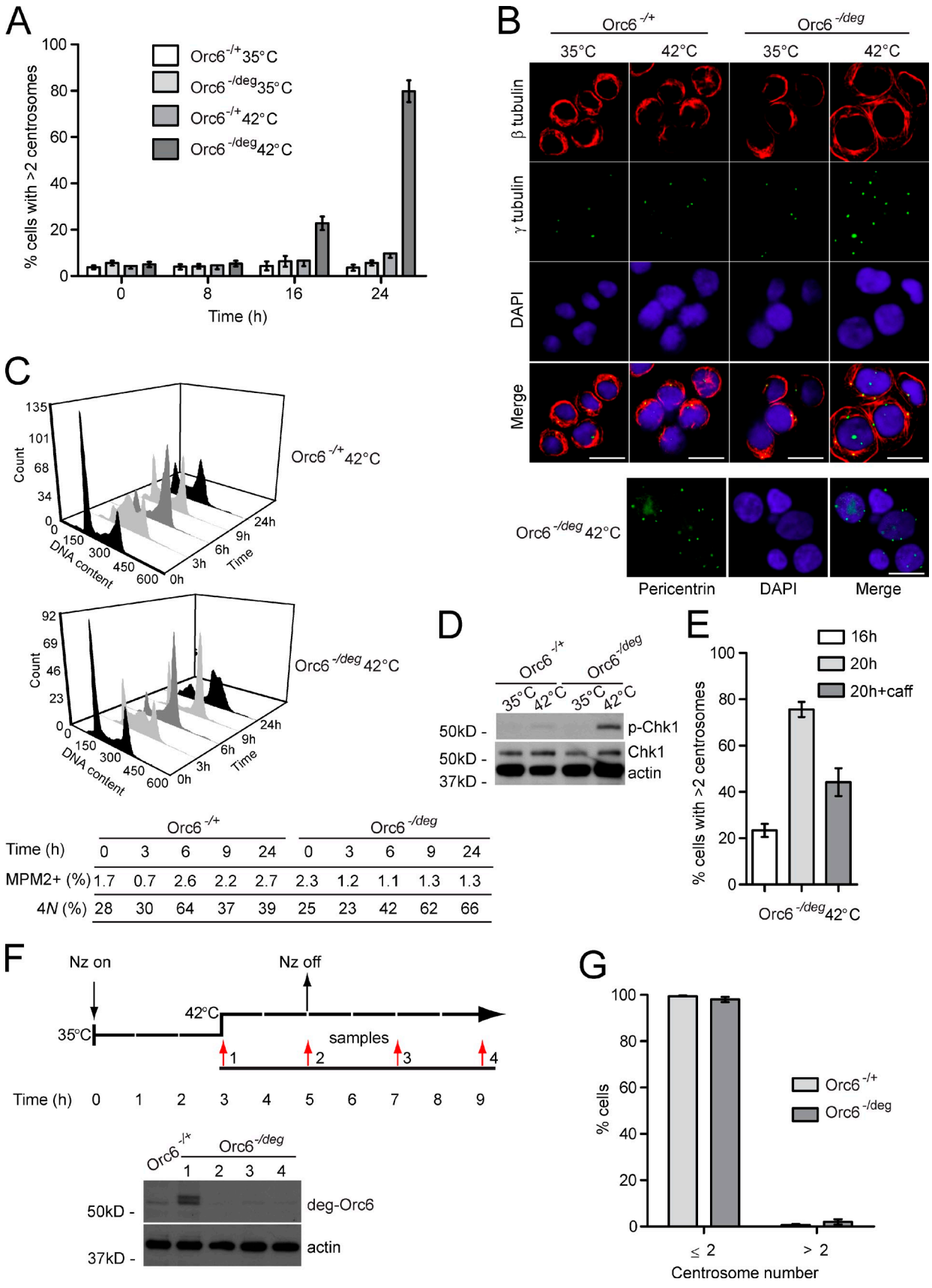

	Orc6 -/+					Orc6 -/deg				
Time (h)	0	3	6	9	24	0	3	6	9	24
MPM2+ (%)	1.7	0.7	2.6	2.2	2.7	2.3	1.2	1.1	1.3	1.3
4*N* (%)	28	30	64	37	39	25	23	42	62	66

Figure 2. **Degron-Orc6 depletion during the S phase triggers supernumerary centrosome formation suppressed by G2 checkpoint inhibition.** (A) Enumeration of cells with multiple anti–γ-tubulin–stained centrosomes. Control cells expressing degron-Orc6 are compared with Orc6$^{-/deg}$ cells lacking Orc6 at different time points after shifting to 42°C. The same cells maintained at 35°C represent controls. At least 200 cells were analyzed per time point. The percentage of cells

from serial time-lapse images show that *Orc6*$^{-/deg}$ cells lacking degron-Orc6 displayed asymmetric cell cleavage and failure in cytokinesis in contrast to the symmetric division of controls (Fig. 3, A–E). Moreover, during cytokinetic furrow ingression, degron-Orc6–depleted cells exhibited cortical blebbing, furrow regression, and failure to divide, forming multinucleated cells (Fig. 3, B and C). Defective cell division was strikingly more frequent in cells lacking full-length degron-Orc6 than in controls (Fig. 3 F, compare *Orc6*$^{-/deg}$ and *Orc6*$^{-/deg/EGFP\text{-}Orc6\Delta25}$ with *Orc6*$^{-/deg}$ and *Orc6*$^{-/deg/EGFP\text{-}Orc6}$). Full-length EGFP-Orc6 could complement these defects in *Orc6*$^{-/deg}$ cells, whereas EGFP alone or the EGFP-Orc6Δ25C mutant could not (Fig. 3, E and F). Thus collectively, our findings show that the C-terminal region of Orc6 is essential during mitosis for the late stages of cell division and, in particular, that it promotes correct abscission and cell separation. However, EGFP-Orc6Δ25C (like EGFP-Orc6) decorates chromosomes from anaphase to telophase independent of cell division fate and also accumulates in interphase nuclei (Fig. 3, G and H), suggesting that mislocalization does not explain its defective function.

Abscission defects late in cytokinesis are difficult to detect by conventional light microscopy. To determine whether degron-Orc6 depletion during early mitosis induces delayed abscission, we used a fluorescence-bleaching approach to test whether there was a cytoplasmic connection between daughter cells transfected with free monomomeric EGFP (Fig. 4 A). We first depleted degron-Orc6 during mitosis (as in Fig. 2 F) and, during division, photobleached EGFP from one daughter cell and measured over time the mean fluorescence intensity (MFI) of EGFP in its partner (Fig. 4 B). As long as a cytoplasmic connection exists between the two cells, the MFI of the unbleached cell will equilibrate with that of its partner (see example in Fig. 4 C). When abscission is complete and no cytoplasmic connection exists, the MFI of the bleached and unbleached cells will not equilibrate (Fig. 4 C). 2 h after release into mitosis, 92% of *Orc*$^{-/+/EGFP}$ cells (n = 25) have completed abscission, whereas only 24% of *Orc6*$^{-/deg/EGFP}$ cells (n = 25) lacking degron-Orc6 did so in the same time frame (Fig. 4 D). To exclude that this difference was not simply the result of delays in mitosis before the abscission step, we measured the precise timing of abscission and the completion of cell separation by modifying a recently developed fluorescence-bleaching assay (Steigemann and Gerlich, 2009; Steigemann et al., 2009). Repeated bleaching of EGFP in one daughter cell decreases the MFI in the unbleached daughter cell for as long as they maintain their cytoplasmic connection. The decrease in MFI terminates after abscission, when the daughter cells separate (Fig. 4 E). When comparing *Orc6*$^{-/+/EGFP}$ and *Orc6*$^{-/deg/EGFP}$ cells, we find a significant delay in the timing of abscission after degron-Orc6 depletion (78 ± 3.8 min, mean ± SEM; n = 15) compared with control cells (44 ± 1.1 min, mean ± SEM; n = 15; Fig. 4, F–H).

This delay could not be explained by the persistence of DNA bridges between the two daughter cells that might impede abscission (Fig. S3, A and B). Moreover, the Aurora B kinase, which delays abscission when chromosome bridges are present (Steigemann et al., 2009), localizes normally to the midbody in degron-Orc6–depleted cells and did not colocalize with DAPI-stained DNA (Fig. S3 B).

How vertebrate Orc6 may regulate cytokinesis is unclear, although we show that a C-terminal region of 25 residues is necessary for abscission. Silencing of the *D. melanogaster* Orc6 orthologue also causes multinuclear cell division; its conserved C-terminal region binds to the septin "peanut" (Chesnokov et al., 2003; Huijbregts et al., 2009). However, we could not detect an interaction between vertebrate Orc6 and the peanut homologue septin 7 (Fig. S3). Thus, vertebrate Orc6 might exert its functions during abscission through a different mechanism.

In summary, we have exploited an N-end rule degron to show that vertebrate Orc6 is necessary during mitosis for symmetric cell division and cytokinetic abscission; this is distinct from its established function in DNA replication. In contrast, our results suggest that centrosome amplification induced by Orc6 depletion reflects an indirect consequence of aberrant replication, rather than the direct role suggested by previous studies (Prasanth et al., 2002; Chesnokov et al., 2003). Thus, our work illustrates the utility of vertebrate N-end rule degrons to unravel complex phenotypes associated with different functions of a single protein during different phases in the cell cycle.

with multiple centrosomes (± SEM) is plotted against time. Statistically significant differences were found between Orc6-deficient cells versus Orc6-proficient cells at 16 and 24 h at 42°C ($P < 0.001$, two-way analysis of variance [ANOVA] followed by Bonferroni's multiple comparison test). (B) Representative immunofluorescence images of asynchronous Orc6$^{-/+}$ and Orc6$^{-/deg}$ cells 24 h after shifting to 42°C compared with cells growing at 35°C. β-Tubulin marks microtubules (first row), anti–γ-tubulin detects centrosomes (second row), DAPI stains DNA (third row), whereas the fourth row shows the merged staining. Multiple centrosomes are abundant in the Orc6-deficient Orc6$^{-/deg}$ cells but not in controls expressing Orc6 protein. Centrosome-specific staining of pericentrin in Orc6-depleted cells is shown as a control. Bars, 10 µm. (C) Cell cycle profiles of Orc6$^{-/+}$ and Orc6$^{-/deg}$ cells at the nonpermissive temperature are shown. DNA content measured by propidium iodide staining is plotted against relative cell number. MPM2-positive staining and 4N DNA content percentages are shown below the histograms. Cells lacking degron-Orc6 transit cell cycle with similar kinetics to cells expressing Orc6, only to arrest with 4N DNA content after 24 h (66%, of which 1.3% express MPM2). At this time, 39% of Orc6$^{-/+}$ control cells are in 4N, of which 2.7% express MPM2, which is typical of wild-type DT40 cells (Kikuchi et al., 2005; Su et al., 2008). (D) Orc6$^{-/deg}$ cells and Orc6$^{-/+}$ were shifted to 42°C or maintained at 35°C for 24 h, and G2 checkpoint activation was measured by phospho-Chk1 accumulation relative to total Chk1. (E) G2 checkpoint inhibition using 2 mM caffeine (caff) for 2 h suppresses centrosome accumulation in Orc6$^{-/deg}$ cells 20 h after shifting to 42°C. Differences between caffeine-treated versus untreated cells at 20 h (44.2 ± 6% vs. 75.6 ± 3.2% have more than two centrosomes) were statistically significant ($P < 0.01$ by one-way ANOVA followed by Bonferroni's multiple comparison after the test). (F and G) Multiple centrosomes do not occur when degron-Orc6 is depleted during mitosis. The panel in F shows the experimental time line at intervals of 1 h per segment. Orc6$^{-/deg}$ cells or Orc6$^{-/+}$ controls at 35°C after 3 h in nocodazole (Nz) were shifted to 42°C to degrade Orc6. Nz-arrested cells released synchronously into mitosis were harvested at different times before and after release. Nz was washed out after 2 h at 42°C. Samples were taken at 3, 5, 7, and 9 h (lanes 1–4, respectively). Western blots show total cell extracts immunoblotted with anti-FLAG and anti–β-actin. Degron-Orc6 in Orc6$^{-/deg}$ cells is completely degraded 3–5 h after Nz release. In G, centrosomes were enumerated by γ-tubulin staining after Nz synchronization and release. Graphs show the mean percentage of cells with supernumerary centrosomes (± SEM) from three separate experiments performed blind (n = 50 mitotic cells per experiment).

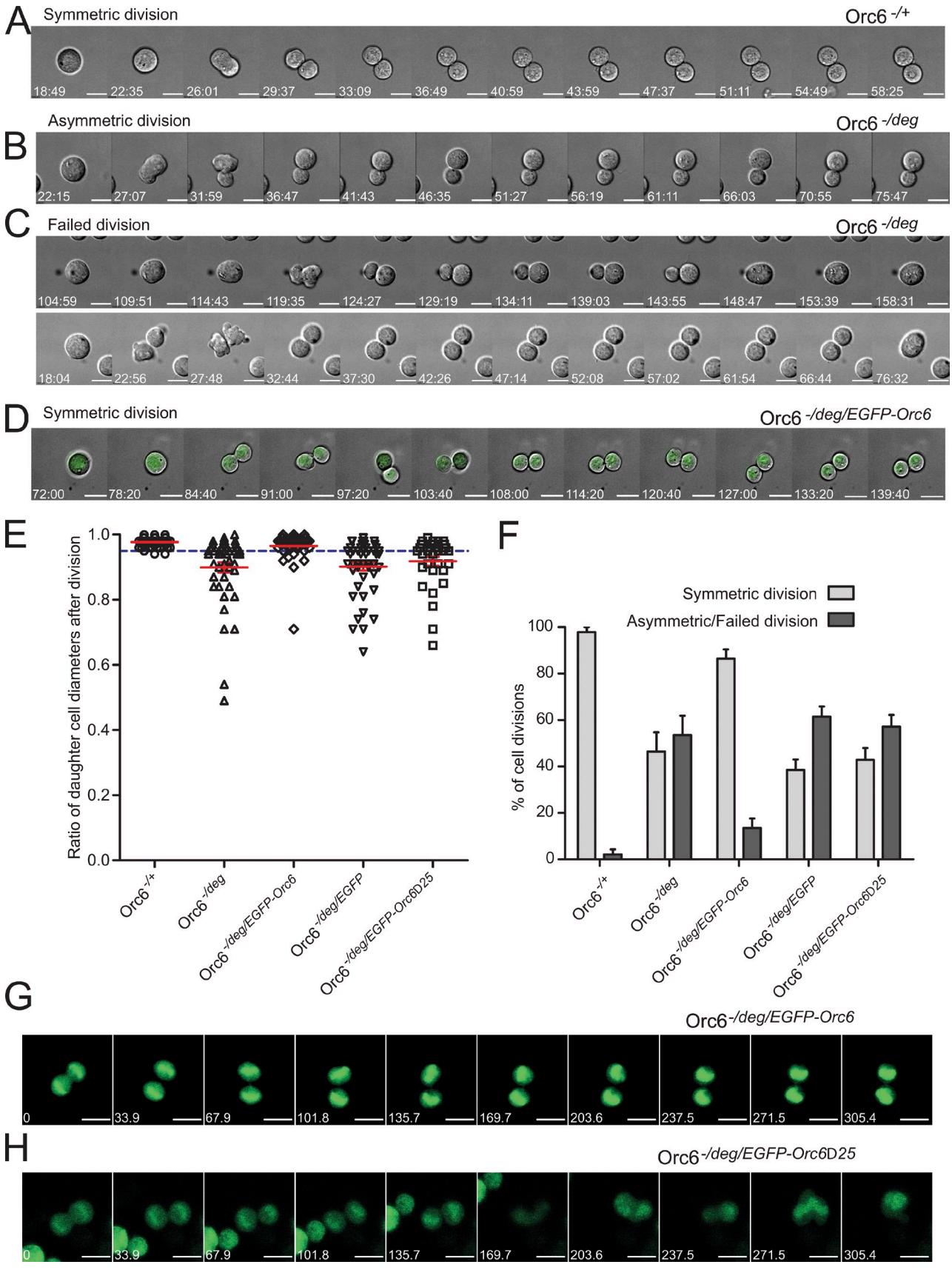

Figure 3. **Degron-Orc6 depletion during mitosis induces asymmetric cell division and failed cytokinesis.** (A–D) Representative mitotic phenotypes in Orc6$^{-/deg}$ cells, Orc6$^{-/deg/EGFP\text{-}Orc6}$, or controls at 42°C. Orc6$^{-/+}$ controls uniformly exhibit symmetric division (A), whereas Orc6$^{-/deg}$ cells exhibit a variety of abnormal phenotypes, including asymmetric division (B) and failed division (C). (D) Symmetric division after reconstitution with Orc6$^{-/deg/EGFP\text{-}Orc6}$.

Our work highlights an evolutionary difference between vertebrate and yeast Orc6 (Fig. 5). Conditional genetic experiments in yeast indicate that yeast Orc6 exclusively functions during DNA replication. In contrast, our findings indicate that Orc6 has acquired an additional and distinct role in the completion of cell division during the transition from unicellular to multicellular organisms, providing fresh insight into the evolution of the mechanisms that coordinate DNA replication and mitosis in eukaryotes.

Materials and methods

Construction of plasmids and targeting vectors

The *Gallus gallus Orc6l* (ENSGALT00000006929, 1261 bp; ENSGALP00000006918, 267 aa) was cloned from DT40 first-strand cDNA by PCR using PF1 and PR1 primers. The PCR product was digested with NotI and KpnI and ligated into *pEGFP-N1* digested with the same enzymes to create *pN1-GgOrc6*. To generate *pEGFP-Orc6* and *pEGFP-Orc6Δ25,* the vector *pEGFP-C1* was digested with EcoRI and KpnI and ligated to the PCR products generated with the primers EGF and EGR1 or EGR2, respectively, cut with the same enzymes.

We created *pDegron-GgOrc6* by PCR amplifying the degron cassette from *pKL187* using the primers *gallus* forward and *gallus* reverse before digestion with NheI and KpnI and ligation into *pN1-GgOrc6*. A targeting vector, pLoxNeo/KO-Orc6, for knocking out the entire *Orc6l* gene, including sequences 2 kb 5′ from the ATG (~6.5 kb in all), was constructed as follows. A left arm from position −4 kb to −2 kb from the ATG (homology A) was amplified by PCR using the primers PF2 and PR2, digested with KpnI and SalI, and ligated into pLoxNeo digested with the same enzymes. This construct was then digested with SpeI and NotI and ligated to a right arm from the 3′ end of the gene to 2 kb downstream (homology B) prepared by PCR using primers PF3 and PR3.

A targeting vector, pLoxBsr/KI-deg-Orc6, for knocking in the *degron* sequence into the endogenous DT40 O*rc6* gene was constructed as follows. A right arm from intron 1 to intron 4 (homology D) was amplified by PCR using the primers PF4 and PR4, digested with SalI, and ligated into pLoxBsr digested with the same enzymes (pLoxBsr-Right-arm). A left arm pLoxBsr/KI-deg-Orc6 was assembled using ZeroBlunt as a backbone in two steps. In the first step, a region from the 3′ end of exon 1 to –2 kb from the ATG (homology C) was amplified using the primers PF5 and PR5 and cloned into Zeroblunt (Invitrogen) to create Zeroblunt-Left-arm. In the second step, the *degron* in frame with the first exon of *Orc6* was amplified using the primer pair PF6 and PR6 and cloned into Zeroblunt-Left-arm using NotI–NdeI. The cassette was digested with NdeI and SpeI and ligated into the pLoxBsr-Right-arm construct as described in this paragraph. All constructs were verified by nucleotide sequencing. Site-directed mutagenesis was used to restore a Kozak sequence 5′ of the ATG.

The following primers were used in this paper (sequences run 5′ to 3′): PF1, ATTGACGGTACCTATGGAGCGCGGCGCGGTCCGGGAG; PR1, TTAATCAGCGGCCGCTTAACCACTGTTTGTCTCTTGTGTCTTAG; PF2, TATGCATGGTACCCAAGGCATGGGCCCTCCAAACAGCACTGAAGC; PR2, TATTCGTCGACAAACGAGGGCGTGTGAGCAAACAGGAGG; PF3, ATTCGAGACTAGTGTCCTTGTGCCTCTAGCTGGCAGTAGGCAGTG; PR3, ATTCATGCGGCCGCTGCCTTTGGCTCAGCTGGGAGGTCGAAAC; PF4, GTCGACGGTGCGGGACTCGGGAGCAAGGAAGGGGTG; PR4, GTCGACGTCCAGCTCCAATCTACACTGACAAGAGAAG; PF5, GCGGCCGCACCACAGCAGAATTGAAGGTAAGCCTGAGGAAC; PR5, CATATGCCCCGCTCTCGGTTCCCGCTCGCTCTGC; PF6, CATATGCAGATTTTCGTCAAGACTTTGACCGGTAAAACCA; PR6, ACTAGTCGGTACCTGACGACGCGCGGCTCGCCGAGCCCCA; *gallus* forward, GGCGCTAGCATGCAGATTTTCGTCAAGA; *gallus* reverse, GGCCGGTACCGAGTCTTTCTTCTCGTAGACTTCAAAC; EGF, ATTCGTGAATTCTATGGAGCGCGGCGCGGTCCGGG; EGR1, TCTAGCGGTACCTTAACCACTGTTTGTCTCTTGTGTCTTAGC; and EGR2, TATGGTACCTTATTCAGTCTTCGGCTGTTTACATGG.

Generation of DT40 cell lines

All targeting constructs were transfected into DT40 as described previously (Su et al., 2008). In brief, 10^6 cells were washed with PBS and resuspended in a final volume of 400 µl PBS. 20 µg of targeting construct was linearized with ApaLI and dissolved in 400 µl PBS. Cells and DNA were mixed in an electroporation cuvette (Bio-Rad Laboratories) and kept on ice for 10 min. Electroporation was performed with an electroporation system (Gene Pulser II; Bio-Rad Laboratories) at 950 µF and 250 V followed by a 10-min incubation on ice. Cells were seeded into five 96-well plates, and the relevant antibiotics were added 24 h later at final concentrations of 1.5 mg/ml G418 (Invitrogen) and 30 µg/ml blasticidin (InvivoGen). *Orc6*$^{+/-}$ *and Orc6*$^{+/deg}$ cells were generated by sequential transfection of pLoxNeo/KO-Orc6 and pLoxBsr/KI-deg-Orc6 targeting constructs into wild-type DT40 cells. Genomic DNA was extracted from the candidate clones by DNAzol (Invitrogen) according to the manufacturer's instructions, and the identification of successful targeting events was performed by PCR product analysis generated by primers 5′ knockout forward (KOF) and 5′ knockout reverse (KOR; 5′ in the knockout) and 3′KOF and 3′KOR (3′ in the knockout) for the heterozygous allele. Degron-positive clones were reselected 2 wk later by their ability to grow at 35°C and lack of viability at 42°C under neomycin and blasticidin selection. These knockin clones were identified using the primers 5′ knockin forward (KIF) and 5′ knockin reverse (KIR; 5′ in the knockin) and 3′KIF and 3′KIR (3′ in the knockin).

The resistance cassettes were then floxed out by transient expression of Cre recombinase. In brief, cells were transfected with the *pPGK-Cre* plasmid (gift from K.J. Patel, Laboratory of Molecular Biology, Cambridge, England, UK) using solution from Nucleofector Kit T (Lonza) according to the manufacturer's guidelines. Clones with restored sensitivity to *Bsr* and *Neo* were selected. Direct sequencing of the RT-PCR product of the observed clone was used to confirm fusion *degron-Orc6* expression. Cells stably expressing *EGFP-Orc6* or *EGFP* were transfected as described in this paper and selected with 1.5 mg/ml G418.

The following primers were used in this paper (sequences run 5′ to 3′): 5′KOF, TGCTTGGAGTTCCCATAAGCATCTTTTAAGG; 5′KOR, GCCTTCTATCGCCTTCTTGACGAGTTCT; 3′KOF, GAGAGCAAGTTAGCTCTGCTAATCA; 3′KOR, AACGCACGGGTGTTGGGTCGTTTGTTC; 5′KIF, TAGCAATGCTCTGCAGGTGGCTAA; 5′KIR, TGCCTACCACCTCTTAGCCTTAGC; 3′KIF, TATACGAACGGTAGGGGATCCAAG; and 3′KIR, AGGTGCTCATAGCAGCAGCTATTC.

Cell culture and viability assay

DT40 cells were maintained in RPMI 1640 medium (Invitrogen) supplemented with 10^{-5} M β-mercaptoethanol, 10% fetal calf serum, and 5% chicken serum (Invitrogen) between 35 and 42°C. DT40 cells were synchronized at early mitosis by the addition of 500 ng/ml^{-1} Nz (Sigma-Aldrich) for 5 h or at the G1/S boundary by exposure to 400 µM mimosine (Sigma-Aldrich) for 5 h (Su et al., 2008). Cells were released by washing

(E) Quantitative analysis from four independent experiments of the asymmetry of cell division by comparison of the diameters of the daughter cells. The blue dotted line representing a ratio of 0.949 (the larger of the two diameters was always used as the denominator) marks the threshold for asymmetry and is twice the standard deviation from the mean ratio for control cells. Comparisons were performed between Orc6$^{-/+}$ controls (n = 51) and cell lines expressing degron-Orc6 (n = 46 that completed division), degron-Orc6, and EGFP (n = 47) and controls expressing degron-Orc6 and EGFP-Orc6 (n = 46) or EGFP-Orc6Δ25 (n = 33) fusion proteins. The mean ratio of daughter cell diameters in Orc6$^{-/+}$ controls was consistently different from that in degron-Orc6–depleted cell lines (0.97 in Orc6$^{-/+}$ controls vs. 0.89 ± 0.01 in Orc6$^{-/deg}$ cells or 0.90 ± 0.01 in Orc6$^{-/deg/EGFP}$ cells). This was reversed by the expression of a functional EGFP-Orc6 protein in Orc6$^{-/deg/EGFP\text{-}Orc6}$ cells (0.97 vs. 0.96 ± 0.01 in Orc6$^{-/deg/EGFP\text{-}Orc6}$ cells) but not with EGFP-Orc6Δ25 (0.97 vs. 0.92 ± 0.01 in Orc6$^{-/deg/EGFP\text{-}Orc6\Delta25}$ cells). These differences were all statistically significant ($P < 0.01$ by one-way ANOVA followed by Bonferroni's multiple comparison after the test). The red lines represent the means ± SEM. (F) The graph represents the contingency table from four independent experiments, with bars showing means ± SEM. Cell lines are significantly different when evaluated by χ^2 test ($P < 0.0001$). Cells expressing a functional form of Orc6 (i.e., Orc6$^{-/+}$ or Orc6$^{-/deg/EGFP\text{-}Orc6}$) exhibit few asymmetric or failed divisions (4%, n = 51; and 15%, n = 48), in contrast to cells expressing degron-Orc6 that is degraded during mitosis (Orc6$^{-/deg}$ [55%, n = 62], Orc6$^{-/deg/EGFP}$ [63%, n = 56], or Orc6$^{-/deg/EGFP\text{-}Orc6\Delta25}$ [58%, n = 48] cells). (G and H) Representative frames from a time-lapse confocal series of Orc6$^{-/deg/EGFP\text{-}Orc6}$ or Orc6$^{-/+/EGFP\text{-}Orc6\Delta25}$ cells at 42°C showing EGFP-Orc6 localization at late mitosis. Numbers indicate elapsed time in seconds. Bars, 10 µm. Images were typical of EGFP-Orc6 and EGFP-Orc6Δ25 localization in 10 cells from three independent samples.

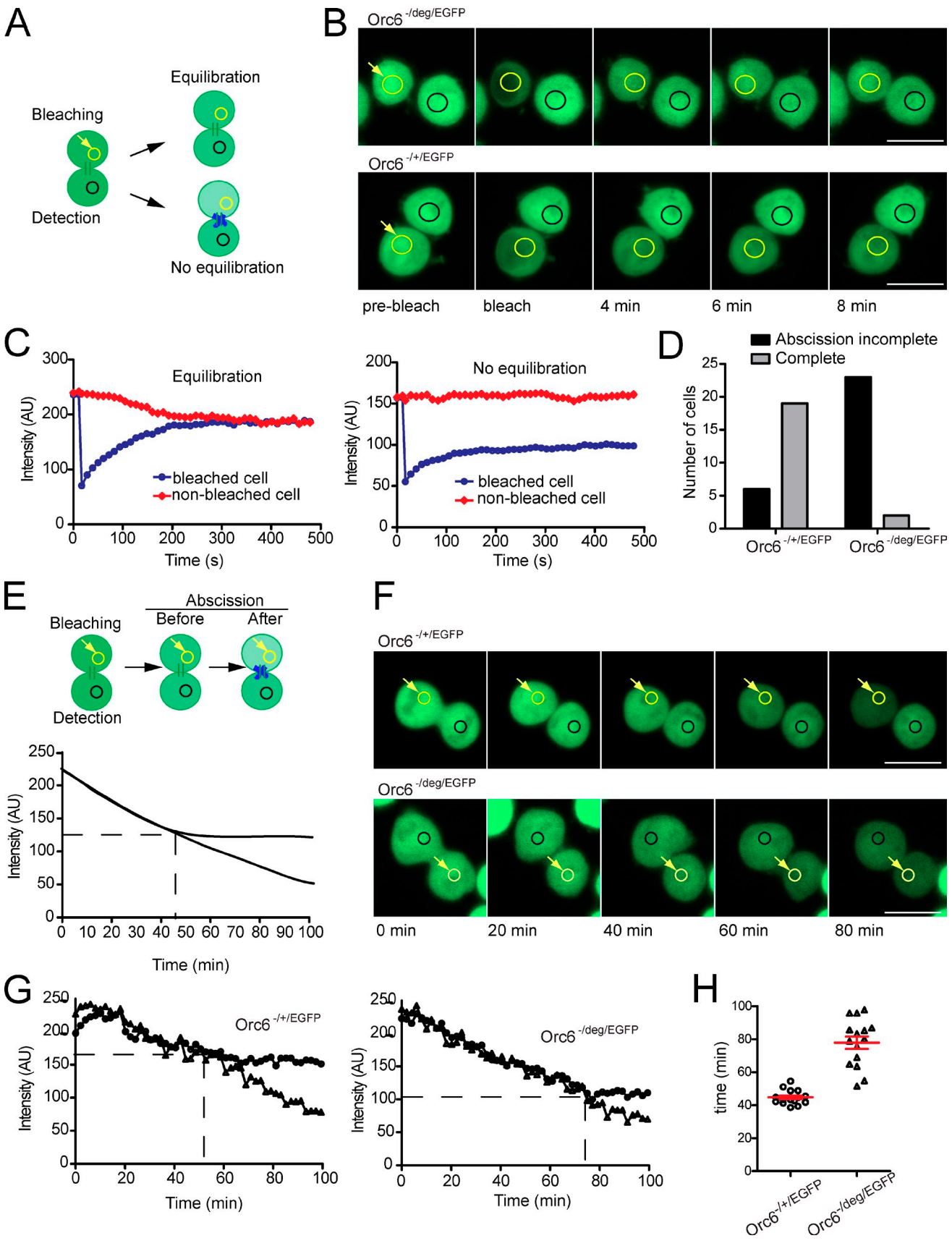

Figure 4. **Degron-Orc6 depletion during mitosis delays in cell abscission.** (A) Experimental design for the diffusion-based fluorescence-bleaching assay to detect the completion of cytokinetic abscission. (B) Selected frames from time-lapse series of Orc6$^{-/deg/EGFP}$ cells (expressing degron-Orc6 and EGFP) or Orc6$^{-/+/EGFP}$ controls (expressing wild-type Orc6 and EGFP) after synchronization and release from Nz. Free EGFP was bleached from one of the two daughter

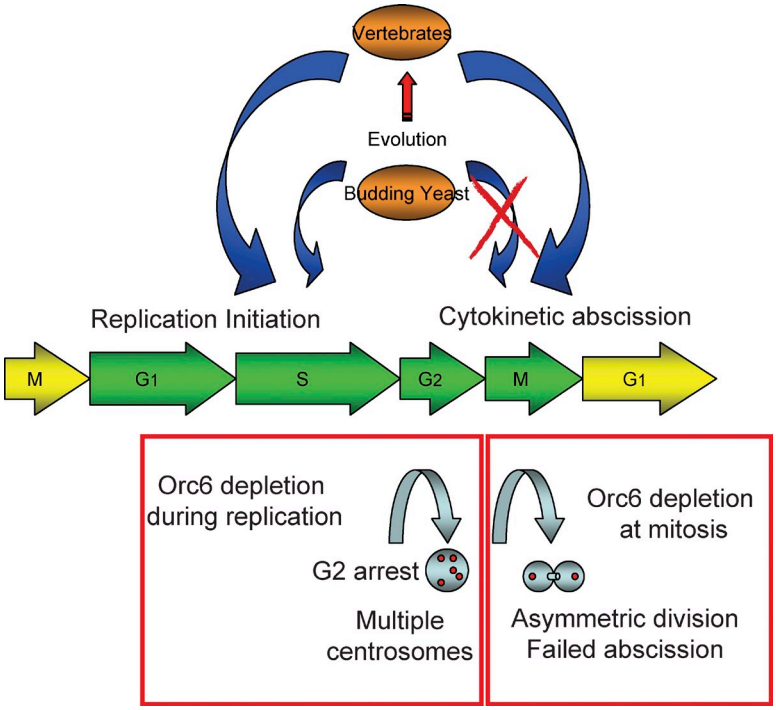

Figure 5. **Distinct contributions of Orc6 to normal mitosis in vertebrate cells versus budding yeast.** In budding yeast, Orc6 functions exclusively in DNA replication, whereas in vertebrate cells, it has acquired a distinct role in promoting symmetric cell division and the abscission step of cytokinesis independent of DNA replication. Other cell cycle abnormalities (e.g., supernumerary centrosome formation) triggered by Orc6 inactivation during the S phase stem indirectly from the cellular response to aberrant replication.

three times with warm media, and samples were taken after release at the time points indicated in the figures. Caffeine (Sigma-Aldrich) was used at 2 mM for 2 h to suppress the G2 checkpoint. The doubling time of DT40 cells was determined by counting the viable cell number enumerated after trypan blue staining with a cell viability analyzer (Vi-CELL; Beckman Coulter) according to the manufacturer's guidelines.

Cell cycle analysis

DT40 cells (2×10^6) were resuspended in 0.5 ml PBS before addition of 4.5 ml of ice-cold 70% (vol/vol) EtOH and incubation for ≥2 h. Before analysis, cells were washed once with PBS and stained with anti-MPM2 antibody (1:1,200; Upstate Cell Signaling) for 1 h at 37°C before washing and staining with Alexa Fluor 488–conjugated secondary antibody (1:500) for 1 h at room temperature. Cells were incubated in 1 ml of 20 mg/ml^{-1} propidium iodide (Sigma-Aldrich), 50 mg/ml^{-1} RNase A, and 0.1% (vol/vol) Triton X-100 in PBS for 15 min at 37°C. Cell cycle profiles were acquired on a flow cytometer (FACSCalibur; BD) using FACSDiva software 6.0 (BD).

Immunodetection and antibodies

Immunofluorescence analyses were performed as described previously (Su et al., 2008). In brief, ∼10^5 cells were spun out onto glass slides in a Cytospin-2 cytocentrifuge (Shandon) for 5 min at 800 rpm. Slides were dried at 37°C for 5 min and fixed in 4% paraformaldehyde for 15 min at room temperature or directly in 100% MeOH at −20°C. Subsequently, slides were then rinsed in PBS and kept at −20°C in 70% EtOH until further analysis. Cells were blocked with 3% BSA in PBS, 0.01% Tween 20, and 0.01% Triton X-100, stained with primary antibodies (mouse anti–β-tubulin [Sigma-Aldrich], rabbit anti–Aurora B [ab2254], rabbit antipericentrin [ab4448; Abcam], or rabbit anti–γ-tubulin [Sigma-Aldrich]) followed by Alexa Fluor 488 or Alexa Fluor 568 secondary antibodies (Invitrogen), and mounted in Vectashield medium with DAPI (Vector Laboratories). Imaging was performed on a confocal microscope (LSM 510 Meta; Carl Zeiss, Inc.) using a 63× Apochromat 1.4 NA objective. For Western blotting, total cell extracts were prepared in ice-cold radioimmunoprecipitation assay buffer (50 mM Tris-HCl, pH 7.4, 150 mM NaCl, 0.5% [vol/vol] deoxycholate, 0.1% [vol/vol] SDS, and 1% [vol/vol] Nonidet P-40) supplemented with 1 mM DTT, 1 mM PMSF, and protease inhibitors (GE Healthcare). For fractionation, cells were lysed with buffer A (10 mM Hepes, pH 7.9, 10 mM KCl, 1.5 mM $MgCl_2$, 0.034 M sucrose, 10% glycerol, 1 mM DTT, 100 µM PMSF, protease inhibitor cocktail [Complete; Roche], 5 mM Na_3VO_4, 10 mM NaF, and 1 µM okadaic acid) with 0.1% Triton X-100 for 5 min on ice. Cells were centrifuged at 1,300 *g* for 4 min, and the supernatant was collected as a soluble cytoplasmic protein. This fraction was further clarified by high speed centrifugation. The nuclei were washed in buffer A and then lysed by buffer B (3 mM EDTA, 0.2 mM EGTA, 1 mM DTT, PMSF, Complete protease inhibitor cocktail, 5 mM Na_3VO_4, 10 mM NaF, and 1 µM okadaic acid) for 1 min on ice. Nuclei were centrifuged at 1,700 *g*

cells (yellow arrow and circle) at t = 0 min. Changes in EGFP fluorescence were then measured in the nonbleached daughter cell (black circle). Before abscission, there is a loss of EGFP fluorescence in the nonbleached daughter caused by a free exchange of EGFP between the connected daughters. After abscission is completed, there is no such loss because the cytoplasm of the daughter cells has been separated. (C) MFI in the regions of interest in bleached and nonbleached cells from a single representative experiment is plotted in arbitrary units (AU). In connected cells (left) MFI equilibrates between the two daughter cells in contrast to cells that have completed the abscission step of cytokinesis (right). (D) Degron-Orc6 depletion increases the proportion of cells that fail to complete abscission 2 h after Nz release. The graph represents values from the contingency tables from five independent experiments ($n = 25$ divisions per cell line). The differences are statistically significant ($P < 0.0001$ by two-tailed Fisher's exact test). (E) Experimental design for an assay to determine the time taken to complete abscission. From t = 0 min corresponding to the time of complete cleavage furrow ingression, one daughter cell was subjected to repeated partial fluorescence bleaching, and EGFP MFI was measured in both the bleached and the nonbleached daughter. The curves show the gradual decline in EGFP MFI in both cells before abscission has been completed. There is a marked inflection in the curve corresponding to the nonbleached daughter, with a stabilized MFI, when abscission is complete. The dashed lines show the inflection point, which represents the time taken from t = 0 min to complete abscission. (F) In $Orc6^{-/+/EGFP}$ controls at 42°C, the decline in EGFP MFI is stabilized ∼40–60 min after complete furrow ingression (top row). However, in $Orc6^{-/deg/EGFP}$ cells at 42°C, the decline in EGFP MFI continues for ≥80 min (bottom row). (G) Graphical representation as explained in E of the MFI curves for a single representative experiment performed in $Orc6^{-/+/EGFP}$ controls (left) or $Orc6^{-/deg/EGFP}$ cells (right). Cessation of the decrease in MFI in the nonbleached cell marks the time taken to complete abscission (dashed lines). (H) Dot plot representing the time distribution for completion of abscission determined from eight independent experiments. The mean time taken to complete abscission is 44.8 ± 1.1 min (means ± SEM, red lines) for $Orc6^{-/+/EGFP}$ controls ($n = 15$) versus 78 ± 3.8 min for $Orc6^{-/deg/EGFP}$ cells ($n = 15$), a difference that is statistically significant ($P < 0.0001$ by two-tailed Mann–Whitney test). Bars, 10 µm.

for 4 min. The soluble nuclear fraction was collected and mixed with the cytoplasmic soluble protein to constitute the soluble fraction. The insoluble chromatin pellet was then resuspended in buffer A with 1 mM $CaCl_2$ and 0.2 U micrococcal nuclease incubated at 37°C for 10 min. The chromatin fraction was collected by high speed centrifugation. Protein concentration was quantified using the bicinchoninic acid assay (Sigma-Aldrich). Cell extracts were resolved by 4–12% SDS-PAGE (Invitrogen) and transferred to nylon membranes (Millipore) before blotting with the appropriate antibodies (anti-EGFP [JL-18; BD], anti-Mek2 [BD], anti–histone H3 [Cell Signaling Technology], anti-FLAG [M2; Sigma-Aldrich], anti-CHK1 [G-4], septin 7 [H-120; Santa Cruz Biotechnology, Inc.], anti-Mcm2 [ab4461; Abcam], anti–phospho-CHK1 [S345; Cell Signaling Technology], or anti–β-actin [Sigma-Aldrich]). HRP-conjugated secondary antibodies against rabbit and mouse were used at 1:20,000 or 1:40,000 dilutions, respectively. Signal intensities were quantified by integrated density measurements on ImageJ (National Institutes of Health).

Live-cell microscopy

Cells were plated in glass-bottomed Mat-Tek dishes. Before imaging, growth medium was replaced with phenol red–free L15 imaging medium. Confocal live imaging was performed on a customized microscope (LSM 510 Axiovert; Carl Zeiss, Inc.) using a 100× 1.4 NA oil Plan Apochromat objective (Carl Zeiss, Inc.) or a microscope (IX81; Olympus) using a 40× 1.4 NA objective. Both microscopes were equipped with piezo focus drives and incubation chambers, providing a humidified atmosphere at 35 or 42°C. Long-term videos for Fig. 3 were acquired on an IX81 microscope (CellR software). Sample illumination was kept to a minimum and had no adverse effect on cell division and proliferation. Image analysis was preformed by LSM 510 and ImageJ software. No contrast adjustments were applied.

FRAP and fluorescence loss in photobleaching

For experiments shown in Fig. 4, EGFP was bleached by radiating a defined region with a 488-nm laser at 100% transmission. Bleaching of EGFP on a microscope (LSM 510) was preformed by epifluorescence illumination. FRAP experiments used 50 iterations of photobleaching at 100% transmission of a 488-nm Ar ion laser at a 15-mW output at regions similar to the one indicated in Fig. 4 A. The recovery kinetics of MFI was measured in a region of constant size. Fluorescence loss in photobleaching experiments used 20 iterations of photobleaching at 100% transmission of a 488-nm laser at regions similar to the one indicated in Fig. 4 D. Bleaching was repeated every five cycles of 120 s. Mean fluorescence was measured in regions of constant size as indicated in Fig. 4 D.

Quantitative immunofluorescence microscopy

Cells cytospun onto glass slides were stained with rabbit polyclonal anti–γ-tubulin and detected using an Alexa Fluor 488–conjugated anti–rabbit antibody. Slides were mounted with Vectashield medium. 20 representative fields were acquired using a 40× 1.4 NA objective on a confocal microscope (LSM 510 Meta) for each sample using constant zoom and imaging parameters (laser intensities and detector settings). Typically, 50–200 cells were analyzed in each sample to determine parameters, including mean number of foci per cell and number of cells with more than a defined foci count. Cells containing more than two γ-tubulin foci were counted as positive for supernumerary centrosomes. The data were plotted in Prism v5.0 (GraphPad Software).

Statistical analyses

All statistical analyses were performed using Prism v5.0 for Windows (Microsoft).

Immunoprecipitations

Immunoprecipitations were performed from 1 mg lysate using 4 µg of control mouse IgG (Sigma-Aldrich) or mouse anti-EGFP (Abcam). Immune complexes were captured on protein A–Sepharose (GE Healthcare). Whole-cell extracts and immunoprecipitates were resolved by 4–12% gradient SDS-PAGE, transferred to nylon membranes (Immobilon-P; Millipore), and blotted with polyclonal antisera against EGFP (Takara Bio Inc.) or septin 7.

Online supplemental material

Fig. S1 shows the generation and characterization of a cell line expressing functional degron-Orc6. Fig. S2 shows that degron-RAD51 depletion during the S phase triggers supernumerary centrosome formation. Fig. S3. shows that abscission defects after Orc6 depletion correlate neither with abnormal DNA bridges during division nor an interaction with septin 7. Online supplemental material is available at http://www.jcb.org/cgi/content/full/jcb.201008125/DC1.

We thank the members of the Venkitaraman laboratory for helpful discussion and technical advice and Dr. K.J. Patel for the gift of reagents.

This work was supported by grants to A.R. Venkitaraman from the Wellcome Trust and the Medical Research Council. J.A. Bernal was also supported by the Spanish Ramón y Cajal program (RYC-2009-04341) from the Ministry of Science and Innovation.

Submitted: 23 August 2010
Accepted: 18 February 2011

References

Balasov, M., R.P. Huijbregts, and I. Chesnokov. 2009. Functional analysis of an Orc6 mutant in *Drosophila*. *Proc. Natl. Acad. Sci. USA*. 106:10672–10677. doi:10.1073/pnas.0902670106

Bell, S.P. 2002. The origin recognition complex: from simple origins to complex functions. *Genes Dev.* 16:659–672. doi:10.1101/gad.969602

Bell, S.P., and B. Stillman. 1992. ATP-dependent recognition of eukaryotic origins of DNA replication by a multiprotein complex. *Nature*. 357:128–134. doi:10.1038/357128a0

Bell, S.P., J. Mitchell, J. Leber, R. Kobayashi, and B. Stillman. 1995. The multidomain structure of Orc1p reveals similarity to regulators of DNA replication and transcriptional silencing. *Cell*. 83:563–568. doi:10.1016/0092-8674(95)90096-9

Chesnokov, I.N. 2007. Multiple functions of the origin recognition complex. *Int. Rev. Cytol.* 256:69–109. doi:10.1016/S0074-7696(07)56003-1

Chesnokov, I.N., O.N. Chesnokova, and M. Botchan. 2003. A cytokinetic function of *Drosophila* ORC6 protein resides in a domain distinct from its replication activity. *Proc. Natl. Acad. Sci. USA*. 100:9150–9155. doi:10.1073/pnas.1633580100

Dhar, S.K., and A. Dutta. 2000. Identification and characterization of the human ORC6 homolog. *J. Biol. Chem.* 275:34983–34988. doi:10.1074/jbc.M006069200

Dodson, H., E. Bourke, L.J. Jeffers, P. Vagnarelli, E. Sonoda, S. Takeda, W.C. Earnshaw, A. Merdes, and C. Morrison. 2004. Centrosome amplification induced by DNA damage occurs during a prolonged G2 phase and involves ATM. *EMBO J.* 23:3864–3873. doi:10.1038/sj.emboj.7600393

Dohmen, R.J., and A. Varshavsky. 2005. Heat-inducible degron and the making of conditional mutants. *Methods Enzymol.* 399:799–822. doi:10.1016/S0076-6879(05)99052-6

Dohmen, R.J., P. Wu, and A. Varshavsky. 1994. Heat-inducible degron: a method for constructing temperature-sensitive mutants. *Science*. 263:1273–1276. doi:10.1126/science.8122109

Duncker, B.P., I.N. Chesnokov, and B.J. McConkey. 2009. The origin recognition complex protein family. *Genome Biol.* 10:214. doi:10.1186/gb-2009-10-3-214

Gillespie, P.J., A. Li, and J.J. Blow. 2001. Reconstitution of licensed replication origins on *Xenopus* sperm nuclei using purified proteins. *BMC Biochem.* 2:15. doi:10.1186/1471-2091-2-15

Gossen, M., D.T. Pak, S.K. Hansen, J.K. Acharya, and M.R. Botchan. 1995. A *Drosophila* homolog of the yeast origin recognition complex. *Science*. 270:1674–1677. doi:10.1126/science.270.5242.1674

Heffernan, T.P., D.A. Simpson, A.R. Frank, A.N. Heinloth, R.S. Paules, M. Cordeiro-Stone, and W.K. Kaufmann. 2002. An ATR- and Chk1-dependent S checkpoint inhibits replicon initiation following UVC-induced DNA damage. *Mol. Cell. Biol.* 22:8552–8561. doi:10.1128/MCB.22.24.8552-8561.2002

Huijbregts, R.P., A. Svitin, M.W. Stinnett, M.B. Renfrow, and I. Chesnokov. 2009. *Drosophila* Orc6 facilitates GTPase activity and filament formation of the septin complex. *Mol. Biol. Cell*. 20:270–281. doi:10.1091/mbc.E08-07-0754

Kikuchi, K., Y. Taniguchi, A. Hatanaka, E. Sonoda, H. Hochegger, N. Adachi, Y. Matsuzaki, H. Koyama, D.C. van Gent, M. Jasin, and S. Takeda. 2005. Fen-1 facilitates homologous recombination by removing divergent sequences at DNA break ends. *Mol. Cell. Biol.* 25:6948–6955. doi:10.1128/MCB.25.16.6948-6955.2005

Labib, K., J.A. Tercero, and J.F. Diffley. 2000. Uninterrupted MCM2-7 function required for DNA replication fork progression. *Science*. 288:1643–1647. doi:10.1126/science.288.5471.1643

Li, J.J., and I. Herskowitz. 1993. Isolation of ORC6, a component of the yeast origin recognition complex by a one-hybrid system. *Science*. 262:1870–1874. doi:10.1126/science.8266075

Li, Y., and J.B. Dodgson. 1995. The chicken HMG-17 gene is dispensable for cell growth in vitro. *Mol. Cell. Biol.* 15:5516–5523.

Meraldi, P., R. Honda, and E.A. Nigg. 2002. Aurora-A overexpression reveals tetraploidization as a major route to centrosome amplification in p53−/− cells. *EMBO J.* 21:483–492. doi:10.1093/emboj/21.4.483

Pak, D.T., M. Pflumm, I. Chesnokov, D.W. Huang, R. Kellum, J. Marr, P. Romanowski, and M.R. Botchan. 1997. Association of the origin recognition complex with heterochromatin and HP1 in higher eukaryotes. *Cell*. 91:311–323. doi:10.1016/S0092-8674(00)80415-8

Prasanth, S.G., K.V. Prasanth, and B. Stillman. 2002. Orc6 involved in DNA replication, chromosome segregation, and cytokinesis. *Science*. 297:1026–1031. doi:10.1126/science.1072802

Prasanth, S.G., K.V. Prasanth, K. Siddiqui, D.L. Spector, and B. Stillman. 2004. Human Orc2 localizes to centrosomes, centromeres and heterochromatin during chromosome inheritance. *EMBO J.* 23:2651–2663. doi:10.1038/sj.emboj.7600255

Quintana, D.G., and A. Dutta. 1999. The metazoan origin recognition complex. *Front. Biosci.* 4:D805–D815. doi:10.2741/Quintana

Rowles, A., and J.J. Blow. 1997. Chromatin proteins involved in the initiation of DNA replication. *Curr. Opin. Genet. Dev.* 7:152–157. doi:10.1016/S0959-437X(97)80123-2

Semple, J.W., L.F. Da-Silva, E.J. Jervis, J. Ah-Kee, H. Al-Attar, L. Kummer, J.J. Heikkila, P. Pasero, and B.P. Duncker. 2006. An essential role for Orc6 in DNA replication through maintenance of pre-replicative complexes. *EMBO J.* 25:5150–5158. doi:10.1038/sj.emboj.7601391

Shimada, K., and S.M. Gasser. 2007. The origin recognition complex functions in sister-chromatid cohesion in *Saccharomyces cerevisiae*. *Cell*. 128:85–99. doi:10.1016/j.cell.2006.11.045

Steigemann, P., and D.W. Gerlich. 2009. Cytokinetic abscission: cellular dynamics at the midbody. *Trends Cell Biol.* 19:606–616. doi:10.1016/j.tcb.2009.07.008

Steigemann, P., C. Wurzenberger, M.H. Schmitz, M. Held, J. Guizetti, S. Maar, and D.W. Gerlich. 2009. Aurora B-mediated abscission checkpoint protects against tetraploidization. *Cell*. 136:473–484. doi:10.1016/j.cell.2008.12.020

Su, X., J.A. Bernal, and A.R. Venkitaraman. 2008. Cell-cycle coordination between DNA replication and recombination revealed by a vertebrate N-end rule degron-Rad51. *Nat. Struct. Mol. Biol.* 15:1049–1058. doi:10.1038/nsmb.1490

Xiao, Z., Z. Chen, A.H. Gunasekera, T.J. Sowin, S.H. Rosenberg, S. Fesik, and H. Zhang. 2003. Chk1 mediates S and G2 arrests through Cdc25A degradation in response to DNA-damaging agents. *J. Biol. Chem.* 278:21767–21773. doi:10.1074/jbc.M300229200